Journal of Molecular Catalysis A: Chemical 326 (2010) 8–14

Contents lists available at ScienceDirect

Journal of Molecular Catalysis A: Chemical

journal homepage: www.elsevier.com/locate/molcata

Editor's choice paper

One-pot hydrothermal synthesis and enhanced photocatalytic activity of trifluoroacetic acid modified TiO_2 hollow microspheres

Jiaguo Yu*, Lei Shi

State Key Laboratory of Advanced Technology for Material Synthesis and Processing, Wuhan University of Technology, Luoshi Road 122#, Wuhan 430070, PR China

ARTICLE INFO

Article history:
Received 26 December 2009
Received in revised form 15 April 2010
Accepted 25 April 2010
Available online 18 May 2010

Keywords:
Titania
Hollow microspheres
Trifluoroacetic acid
Hydrothermal
Surface fluorination
Photocatalytic activity

ABSTRACT

Trifluoroacetic acid (TFA) modified TiO_2 (TFA-TiO_2) hollow microspheres were prepared by one-pot hydrothermal treatment of $Ti(SO_4)_2$ in the presence of TFA at 180 °C for 12 h. The prepared samples were characterized by X-ray diffraction, scanning and transmission electron microscopy, X-ray photoelectron spectroscopy, N_2 adsorption–desorption isotherms and Fourier transform infrared. The production rates of •OH on the surface of UV-illuminated TiO_2 were detected by a photoluminescence (PL) method using terephthalic acid (TA) as probe molecule. The photocatalytic activity was evaluated by the photocatalytic decomposition of acetone in air under UV light illumination. The results show that TFA not only induces the formation of hollow microspheres, but also enhances their crystallization. The molar ratios of TFA to $Ti(SO_4)_2$ (R) have a great influence on photocatalytic activity. When R is in the range of 0.5–5, the photocatalytic activity of the samples is higher than that of commercial Degussa P25 TiO_2 powders (P25) and pure TiO_2 samples. At $R = 2$, the photocatalytic activity of the sample reaches the highest and exceeds that of P25 by a factor of more than two times. This is ascribed to the fact that the former has hollow interior and bimodal mesoporous shells enhancing harvesting of light and the transfer and transport of reactant and product molecules, also, the surface-adsorbed TFA can reduce the recombination of photo-generated electrons and holes.

1. Introduction

In recent years, considerable efforts have been focused on developing highly photoactive oxide semiconductor photocatalysts for their wide application in solar energy conversion and environmental protection since the discovery of photocatalytic water decomposition on TiO_2 electrodes by Fujishima and Honda in 1972 [1–12]. However, the photocatalytic activity of titania should be further enhanced from the practical application and commercial point of view [13–16]. For achieving this purpose, the surface properties and modification of TiO_2 play a very important role in determining photocatalytic reaction efficiencies since heterogeneous photocatalytic reactions usually take place on the surface. It is on the TiO_2 surface that different types of reaction radicals are produced. The most common species is the •OH radical, which can free move to carry out further chemical reaction at the titania surface [17–20]. Recently, F-doping and surface fluorination of TiO_2 have been extensively investigated for enhancing photocatalytic activity [17–36]. Our and other groups' results have indicated that F-doping enhances the crystallization and photocatalytic activity of TiO_2 [22–26]. Furthermore, surface fluorination of TiO_2 has also been used as an effective method for enhanced photocatalytic activity [33–37]. For example, Choi et al. have performed a lot of systemic research works on surface fluorination of TiO_2, and found that surface-fluorinated TiO_2 (F-TiO_2) shows enhanced photocatalytic activities for the photocatalytic oxidation (PCO) of Acid Orange 7 and phenol in aqueous suspensions [17,18]. Also, they found that surface fluorination can be easily performed by a simple ligand exchange reaction between surface hydroxyl groups on TiO_2 and F^- at an acidic environment (ca. pH 3–4) [17]. Minero et al. examined the influence of surface-fluorinated catalysts on the PCO of phenol in aqueous media, and found that the PCO of phenol was enhanced with F-TiO_2 and proposed that the fluorinated surface favors the generation of free •OH radicals (not surface-bound •OH), which are responsible for the enhanced oxidation [29,30]. Since the surface fluorides themselves should not be reactive with valence band (VB) holes [$E^\circ(F^\bullet/F^-) = 3.6$ V vs NHE] [17,32,38]. The higher PCO rate in the F-TiO_2 suspension is ascribed to the enhanced generation of mobile free •OH radicals (reaction (1)) whereas most •OH radicals generated on naked TiO_2 surface prefer to remain adsorbed (reaction (2)) [17].

$$\equiv Ti{-}F + H_2O\,(\text{or}\,OH^-) + h_{vb}{}^+ \rightarrow \equiv Ti{-}F + {}^\bullet OH_{free} + H^+ \quad (1)$$

$$\equiv Ti{-}OH + h_{vb}{}^+ \leftrightarrow \equiv Ti{-}OH^{\bullet +} \quad (2)$$

* Corresponding author. Tel.: +86 27 87871029; fax: +86 27 87879468.
E-mail address: jiaguoyu@yahoo.com (J. Yu).

1381-1169/$ – see front matter © 2010 Elsevier B.V. All rights reserved.
doi:10.1016/j.molcata.2010.04.016

Very recently, we have also reported one-step hydrothermal fabrication of mesoporous surface-fluorinated TiO_2 (F-TiO_2) powders and enhanced photocatalytic activity in photocatalytic oxidation decomposition of acetone in air under UV light illumination, and found that the photocatalytic activity of F-TiO_2 powders is obviously higher than that of pure TiO_2 and commercial Degussa P25 powders due to the fact that the strong electron-withdrawing ability of the surface ≡Ti–F groups reduces the recombination of photo-generated electrons and holes, and enhances the formation of free •OH radicals [37].

To further improve the photocatalytic performance and understand the influence of morphology on photocatalytic activity, various morphological nanostructure TiO_2 have been prepared, including nanotubes, nanorods, nanowires, shuttle-shape nanocrystals or hollow spheres [39–42]. In particular, TiO_2 hollow spheres have caused more and more attention because of their facile mobility, low density, high specific surface areas, and good photocatalytic activity. Up to now, most of the methods for the fabrication of hollow spheres rely on hard or soft sacrificial templates, with the desired hollow interiors generated upon removal of the templates by calcination or dissolution [43,44]. To overcome the disadvantages of the templating method, one-pot template-free methods for hollow structures have been developed based on direct solid evacuation arising from Ostwald ripening, the Kirkendall effect, or chemically induced self-transformation [45–49]. In particular, a great deal of research effort has been devoted to the controlled fabrication of TiO_2 hollow microspheres for their enhanced photocatalytic activity [50–53].

In this work, we fabricate TFA-TiO_2 hollow spheres by one-pot hydrothermal method using $Ti(SO_4)_2$ as precursor and TFA as modifier at 180 °C for 12 h. The influence of R on the morphology and photocatalytic activity of TiO_2 is studied and discussed. To the best of our knowledge, this is the first report on fabrication of TFA-TiO_2 hollow spheres. This work will provide new insights and understanding on the control of morphology and enhancement of photocatalytic activity of TiO_2, and should be of significant interest in solar cell, catalysis, sensing, separation technology, biomedical engineering and nanotechnology.

2. Experimental

2.1. Sample preparation

All chemicals used in this study were of analytical-grade and were used without further purification. Distilled water was used in all experiments. $Ti(SO_4)_2$ was used as titanium source. The pH values of distilled water were adjusted to about 1.3 using a 1.0 M H_2SO_4 solution. Then, 1.5 g of $Ti(SO_4)_2$ and a certain amount of TFA were added into 125 ml of the above mixed solution under vigorous stirring for 1 h. The molar ratio of TFA to $Ti(SO_4)_2$ (R) in the resulting aqueous solution varied from 0, 0.5, 1, 2 to 5. The transparent solution was transferred to a 200-ml Teflon-lined autoclave and then sealed and kept at 180 °C for 12 h. After reaction, the white precipitate obtained was washed with distilled water and ethanol for three times and then dried at 80 °C for 12 h.

2.2. Characterization

Morphological observations were performed by an S-4800 field emission scanning electron microscope (FESEM, Hitachi, Japan) and linked with an Oxford Instruments X-ray analysis system. Transmission electron microscopy (TEM) analyses were conducted by a JEM-2100F electron microscope (JEOL, Japan) using a 200 kV accelerating voltage. X-ray diffraction (XRD) patterns obtained on a D/MAX-RB X-ray diffractometer (Rigaku, Japan) using Cu Kα radiation at a scan rate (2θ) of 0.05° s^{-1} were used to determine the identity of any phase present and their crystallite size. The accelerating voltage and applied current were 40 kV and 80 mA, respectively. The average crystallite size of anatase grains was quantitatively calculated using Scherrer formula ($d = 0.9\lambda/B\cos\theta$, where d, λ, B and θ are crystallite size, Cu Kα wavelength (0.15418 nm), full width at half maximum intensity (FWHM) of (1 0 1) for anatase peak in radians and Bragg's diffraction angle, respectively) after correcting the instrumental broadening. The X-ray photoelectron spectroscopy (XPS) measurement was made in an ultrahigh vacuum VG ESCALAB 210 electron spectrometer equipped with a multichannel detector. All the binding energies were referenced to the C1s peak at 284.8 eV of the surface adventitious carbon. The Brunauer–Emmett–Teller (BET) specific surface area (S_{BET}) of the powders was analyzed by nitrogen adsorption in a Micromeritics ASAP 2020 nitrogen adsorption apparatus (USA). All the samples were degassed at 180 °C prior to nitrogen adsorption measurements. The BET surface area was determined by a multipoint BET method using the adsorption data in the relative pressure (P/P_0) range of 0.05–0.3. A desorption isotherm was used to determine the pore size distribution via the Barret–Joyner–Halender (BJH) method, assuming a cylindrical pore modal [54]. The nitrogen adsorption volume at the relative pressure (P/P_0) of 0.994 was used to determine the pore volume and average pore size. Infrared (IR) spectra on pellets of the samples mixed with KBr were recorded on a Nivolet Magna 560 FTIR spectrometer at a resolution of 4 cm^{-1}. The concentration of the samples was kept at about 0.25–0.3%.

2.3. Analysis of hydroxyl radical (•OH)

Measurements of •OH on the surface of UV-illuminated TiO_2 were performed by the terephthalic acid (TA) fluorescence probe method as follows [55,56]. 0.1 g of TiO_2 powder sample was dispersed in a 20 ml of 5×10^{-4} M TA aqueous solution with a concentration of 2×10^{-3} M NaOH in a dish with a diameter of about 9.0 cm. The experiment was carried out under UV irradiation using a 350 W Xe arc lamp (25 cm above the dishes). The average light intensity striking on the surface of the reaction solution was about 2.0 mW/cm^2, as measured by a UV radiometer (UV-A) with the peak intensity of 365 nm. PL spectra of generated 2-hydroxyterephthalic acid were measured on a Hitachi F-7000 fluorescence spectrophotometer. After UV irradiation for every 15 min, the reaction solution was filtrated to measure the increase in the PL intensity at 425 nm of TAOH excited by 315 nm light [37].

2.4. Measurement of photocatalytic activity

The photocatalytic activity of the samples was measured by the PCO of acetone under UV light irradiation at ambient temperature using a 15 L reactor with an initial acetone concentration of 400 ± 10 ppm [22,37]. A 15 W, 365 nm UV lamp (Cole-Parmer Instrument Co., USA) was used as the light source to trigger the photocatalytic reaction. The TiO_2 photocatalysts were prepared by coating an aqueous suspension of TiO_2 samples onto three dishes with a diameter of 9.0 cm. The dishes were dried in an oven at 100 °C for about 2 h to evaporate the water and then cooled to room temperature before use. The weight of the photocatalyst used for each experiment was kept at about 0.2 g. The acetone vapor was allowed to reach adsorption and desorption equilibrium with the catalyst in the reactor prior to UV light irradiation and each set of experiments were followed for 60 min. The photocatalytic activity of the powders can be quantitatively evaluated by comparing the apparent reaction rate constants. The PCO of acetone is a pseudo-first-order reaction and its kinetics may be expressed as follows: $\ln(C_0/C) = kt$, where k is the apparent reaction rate constant, and C_0

Table 1
Effects of *R* on phase structure, BET surface areas and pore parameters of titania powders.

R	Phase content	Crystalline size (nm)	S_{BET} (m^2/g)	Average pore size	Pore volume (cm^3/g)	Relative crystallinity
0	A	10.8	96.2	6.8	0.21	1.00
0.5	A	11.1	93.2	8.1	0.19	1.03
1	A	11.5	90.6	8.6	0.19	1.07
2	A	12.0	84.3	8.6	0.18	1.11
5	A	13.3	83.4	8.7	0.21	1.23
P25	A, R	20 (A)	55.1	3.9	0.06	–

A and R denote anatase and rutile, respectively.
Relative anatase crystallinity: the relative intensity of the diffraction peak from the anatase (1 0 1) plane (reference: the sample prepared at $R = 0$).

and *C* are the initial concentration and the reaction concentration of acetone, respectively [22,37]. The photocatalytic activity of P25 was also measured as a reference to compare with that of the synthesized catalysts. Each set of photocatalytic measurements was repeated three times, and the experimental error was found to be within ±5%.

3. Results and discussions

3.1. XRD analysis

The XRD patterns in Fig. 1 illustrate the phase structural evolution of the samples prepared at different *R*. It can be seen that the prepared samples consist of well crystallized anatase [JCPDS No. 21-1272, space group: $I4_1/amd$ (1 4 1)] without any impure phase. With increasing *R*, the XRD peak intensities of anatase steadily become stronger and the width becomes slightly narrower, indicating the formation of greater anatase crystallites and the enhancement of crystallization. The average crystalline sizes of the samples are listed in Table 1, indicating that the increasing of *R* results in the increase of crystallite sizes. This result is similar to our previous report that F^- enhances the anatase crystallization and promotes the crystallites coarsening [22,37]. This also implies that the partial decomposition of TFA at high temperatures results in the formation of F^- in the solution. Therefore, it is not surprising that with increasing *R*, crystallization and coarsening of anatase are enhanced due to the formation of more F^-.

3.2. BET surface areas and pore structure

Nitrogen adsorption–desorption isotherms are measured to determine the specific surface areas and pore size distribution curves of TiO_2 samples, and the corresponding results are presented in Fig. 2. It can be observed from Fig. 2a that the nitrogen adsorption–desorption isotherms of pure TiO_2 samples prepared at $R = 0$ are of type IV (Brunauer–Deming–Deming–Teller (BDDT) classification) with two hysteresis loops, implying bimodal pore size distributions in the mesoporous and macroporous region. At low relative pressures between 0.4 and 0.8, the hysteresis loop is of type H2, suggesting the presence of the inkbottle-like pores with narrow necks and wider bodies [54,57,58]. However, at high relative pressures between 0.8 and 1.0, the shape of the hysteresis loop is of type H3, associated with plate-like particles giving rise to slit-like pores [54,57,58]. In addition, with increasing *R*, the hysteresis loops shift slightly to a higher relative pressure region and the area of the hysteresis loops gradually becomes small. Fig. 2b shows corresponding pore size distribution curves of TiO_2 powders prepared at $R = 0$ and 2. Pure TiO_2 powders show small mesopores (ca. 3.5 nm) and large mesopores with a maximum peak pore diameter of ca. 40 nm. According to the previous study [57,58], the

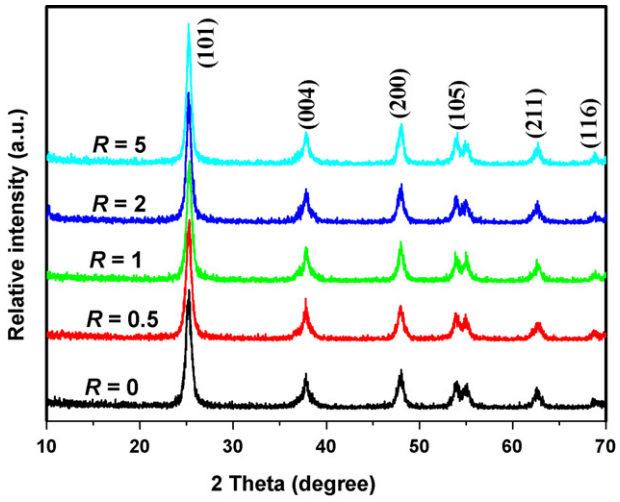

Fig. 1. XRD patterns of TiO_2 samples prepared with varying *R* at 180 °C for 12 h.

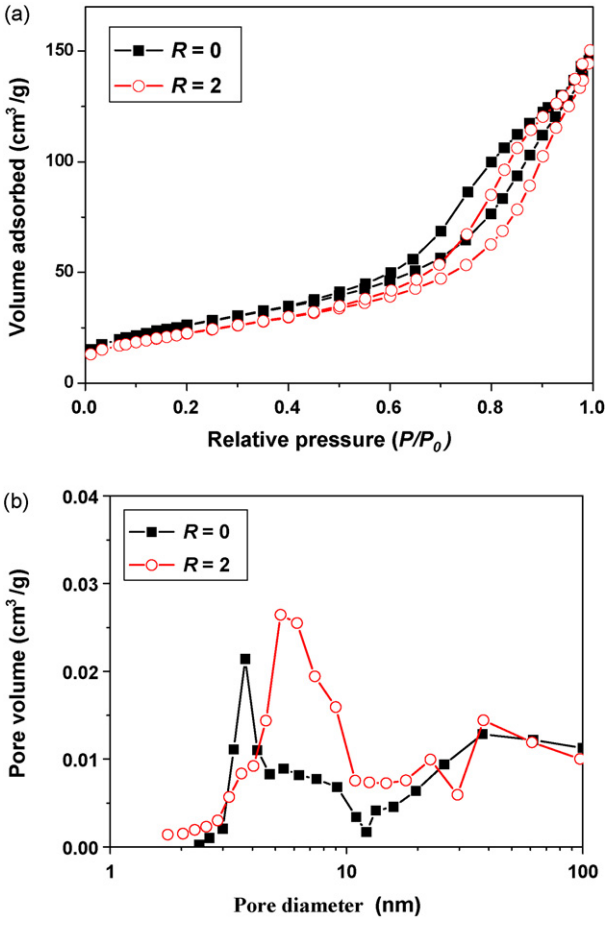

Fig. 2. Nitrogen adsorption–desorption isotherms (a) and corresponding pore size distribution curves (b) of TiO_2 samples prepared at $R = 0$ and 2.

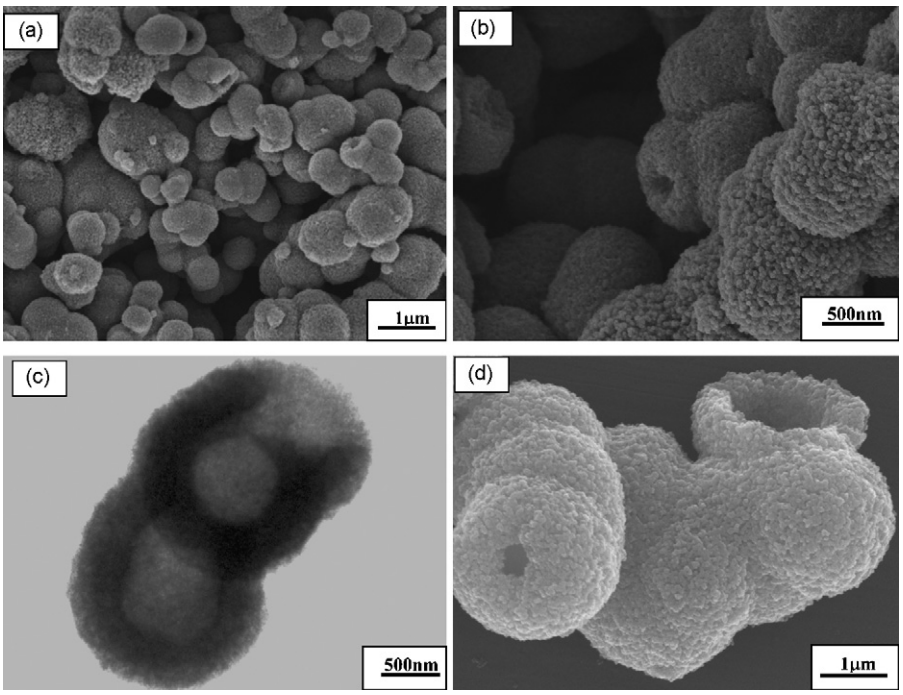

Fig. 3. SEM (a, b, d) and TEM (c) images of TiO_2 samples prepared at $R = 1$ (a), 2 (b, c) and 5 (d).

bimodal mesopore size distribution is from two different aggregates in the powders. The powders contain fine intra-aggregated mesopores formed between intra-agglomerated primary particles (represented by the hysteresis loop in the lower P/P_0 range) and large interaggregated mesopores produced by interaggregated secondary particles (hysteresis loop in the higher P/P_0 range). With increasing R, the peak pore size of intra-particle pore shifts to the right indicating the increase of intra-particle pore size owing to enhanced crystallization and growth of anatase crystallites.

3.3. Morphology aspect

It was reported that hollow microspheres were expected to exhibit a fast motion of charge carriers and enhancement of photocatalytic activity because of their closed packed interpenetrating networks, and large internal surface area [59,60]. As shown in Fig. 3, the morphology and structure of the product are examined by SEM and TEM. In the absence of TFA (in pure water), the samples are solid sphere (not shown here). On the contrary, TiO_2 hollow spheres with diameters of around 500–800 nm can be easily obtained in the presence of TFA. Further observation shows that with increasing R, the diameter of all the samples increases slightly (from ca. 600 nm at $R = 1$–1000 nm at $R = 5$) (see Fig. 3), indicating that the concentration of TFA has a positive effect on the size of hollow spheres. To get more information about the hollow structures, the samples are characterized by TEM. Fig. 3c exhibits the TEM image of the TiO_2 hollow spheres obtained at $R = 2$. The electron-density difference between the dark edge and pale center further confirms the hollow interiors clearly. Localized Ostwald ripening or chemically induced self-transformation mechanism can be used to explain the formation of TiO_2 hollow spheres or hollowing of solid spheres [61,62]. So, it is not difficult to understand that the diameter of hollow spheres is larger than that of TiO_2 solid spheres and the size of hollow spheres increases with increasing R [47–50]. Our previous results have also indicated that fluoride in the acidic condition can promote self-transformation of amorphous TiO_2 solid spheres and formation of TiO_2 hollow spheres [61].

3.4. XPS and IR studies

The surface chemical compositions and chemical states of the samples are further investigated by XPS. XPS survey spectra (not shown here) indicate that all TFA-TiO_2 powders prepared at different R contain Ti, O, C and F elements. Fig. 4 shows high-resolution XPS spectra of F1s region of TFA-TiO_2 samples prepared at $R = 0.5$ and 2. The F1s region consists of two peaks. The main peak at 684.0 eV is ascribed to F^- physically adsorbed on the surface of TiO_2 hollow spheres, while the minor peak at 689.5 eV is associated with C–F bonding of TFA [28]. The former implies that high-temperature hydrothermal decomposition of TFA results in the production of F^-. The latter suggests that some CF_3COO^- anions still exist in the solution. Further observation shows that the relative intensity of the C–F peak from TFA increases with higher R, implying that the

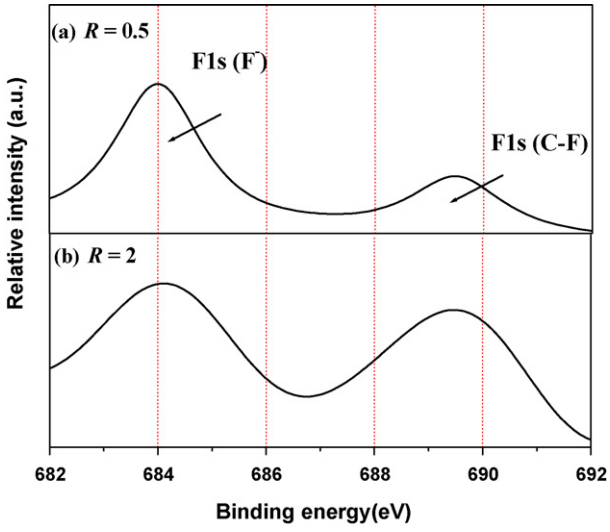

Fig. 4. High-resolution XPS spectra of F1s of TiO_2 hollow microspheres prepared at $R = 0.5$ (a) and 2 (b).

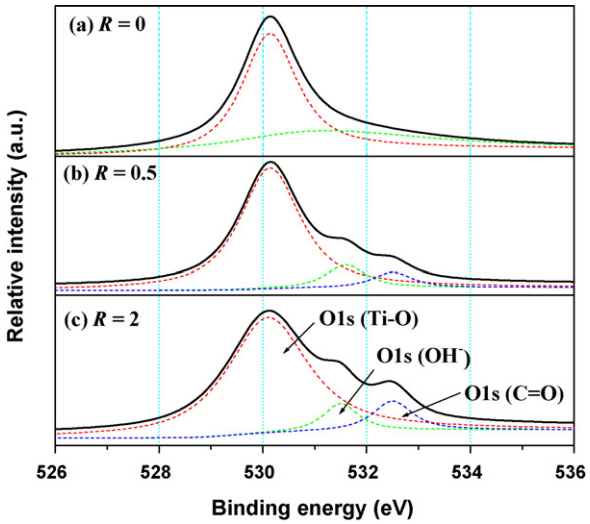

Fig. 5. High-resolution XPS spectra of O1s of TiO_2 samples prepared at $R = 0$ (a), 0.5 (b) and 2 (c).

$R = 2$ samples contain more CF_3 groups due to un-decomposition of more TFA. The above results suggest that there are two kinds of fluorine anions (F^- and CF_3COO^-) adsorbed on the surface of TiO_2 hollow spheres, with increasing R, CF_3COO^- concentration increases. Fig. 5 shows O1s high-resolution XPS spectra of the samples obtained at $R = 0$, 0.5 and 2. The O1s region of pure TiO_2 sample prepared at $R = 0$ (Fig. 5a) can be fitted into two smaller peaks owing to the asymmetric shape of peak. The main peak at 530.0 eV is ascribed to the Ti–O bonds in TiO_2, while the minor peak at 531.5 eV is due to the hydroxyl groups [63–65]. A new peak at 532.6 eV appears for the samples prepared at $R = 0.5$ and 2, which can be ascribed to the carbonyl (C=O) groups of TFA [28]. It is not surprising that an increasing R results in the increase of peak intensity at 532.6 eV. Interestingly, the peak areas of hydroxyl groups of the samples gradually increase with increasing R, indicating that more TFA adsorbed on the surface of TiO_2 also results in the increase of hydroxyl group concentration on TiO_2 surface. This is not difficult to understand because the action of hydrogen bonding of TFA to H_2O will cause the increase of the surface absorbed water. Fig. 6 shows that corresponding high-resolution XPS spectra of C1s region of the samples prepared at $R = 0$, 0.5 and 2. The C1s region of the $R = 2$ sample is fitted into four peaks at 284.9, 285.9, 288.6 and 292.7 eV, which are respectively attributed to the C–C and C–H; C–OH; C=O; and CF_3 groups. The latter three peaks are related to the carbon in the fluorocarbon entities of TFA, also their intensity increases with increasing R. The curve fitting results of XPS spectra of O1s and C1s regions further confirm that with increasing R, more TFA is adsorbed on the surface of TiO_2 through surface complex reaction [28,29].

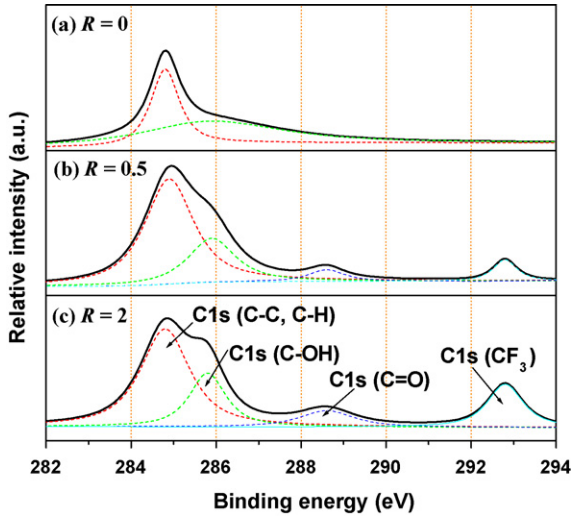

Fig. 6. High-resolution XPS spectra of C1s of TiO_2 samples prepared at $R = 0$ (a), 0.5 (b) and 2 (c).

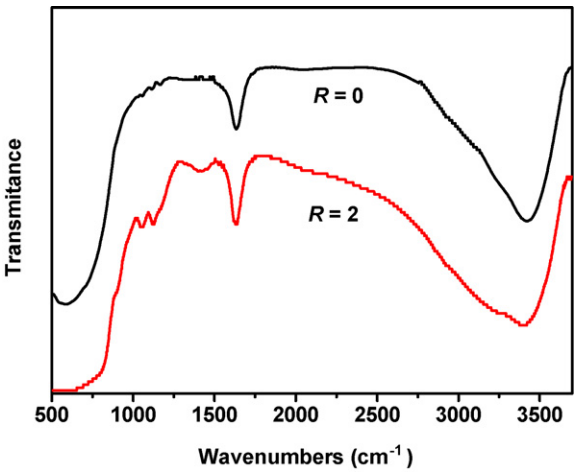

Fig. 7. FTIR spectra of TiO_2 samples prepared at $R = 0$ and 2.

The adsorbed TFA on the surface of TiO_2 is further confirmed by the FTIR spectra. Fig. 7 shows FTIR spectra of TiO_2 prepared at $R = 0$ and 2. The broad peaks at 3400 and 1650 cm^{-1} observed for two TiO_2 samples correspond to the bending and stretching models of surface-adsorbed water and hydroxyl groups, respectively [28,66]. This indicates that water molecules are easily adsorbed on the surface of TiO_2. For TFA-modified TiO_2 sample, two small peaks observed at 1053 and 1140 cm^{-1} in the spectrum are assigned to the C–F stretching vibration of TFA adsorbed on the TiO_2 surface [28]. Further observation indicates that the peaks at 1380–1400 cm^{-1} region are ascribed to carboxyl (C=O) groups, which are also from the surface-bound TFA.

3.5. Hydroxyl radical analysis

The fluorescence emission spectra from TA and TiO_2 mixed solution are measured every 15 min during UV illumination. Fig. 8 shows the changes of fluorescence spectra with irradiation time.

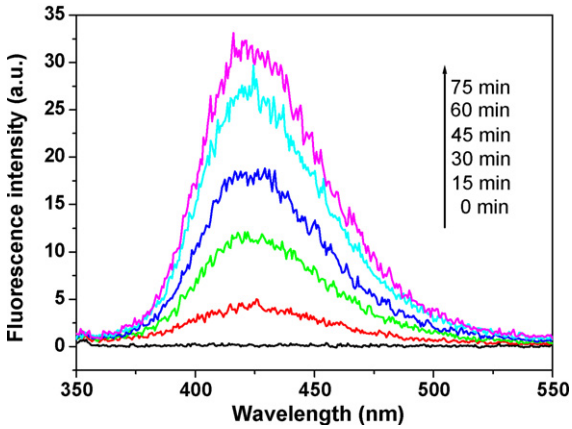

Fig. 8. PL spectral changes observed during illumination of TiO_2 sample prepared at $R = 2$ in a 5×10^{-4} M basic solution of terephthalic acid (excitation at 315 nm). Each fluorescence spectrum was recorded every 15 min of UV illumination.

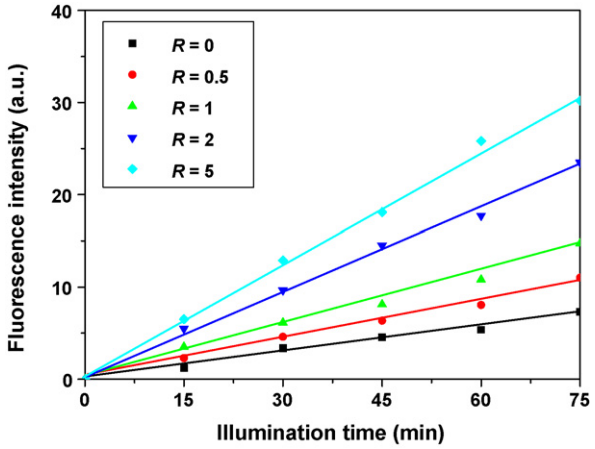

Fig. 9. Plots of the induced PL intensity at 425 nm against irradiation time for the TiO_2 samples prepared at $R = 0$, 0.5, 1, 2 and 5.

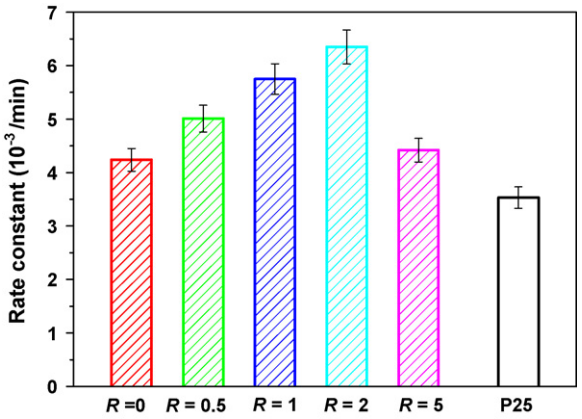

Fig. 10. Comparison of the apparent rate constants of P25 and the TiO_2 samples prepared at different R.

A gradual increase in PL intensity at about 425 nm is observed with increasing irradiation time. However, no PL and PL increase is observed in the absence of UV irradiation or TiO_2 powders. This indicates that PL is from chemical reaction between TA and •OH produced during TiO_2 photocatalytic reaction at the water/TiO_2 interface [55,56]. Fig. 9 shows the dependence of PL intensity at 425 nm on illumination time. It can be seen that the PL intensity linearly increases with time for all the prepared samples. So, it is reasonable to infer that •OH radicals generated via photocatalytic reaction is proportional to irradiation time almost obeying zero-order reaction rate kinetics [55,56]. The formation rate of •OH radicals can be expressed by the slop of these lines shown in Fig. 9. Obviously, the formation rate of •OH radicals in all TFA-TiO_2 samples is much larger than that of pure TiO_2. This can be explained according to our previous suggestion that trifluoroacetate complex or F–Ti groups can capture the photo-generated electrons in the conduction band of TiO_2, thus, reduce the recombination between electrons and holes [28,37]. Consequently, the production rates of •OH radicals are enhanced for all TFA-TiO_2 samples. It is not also difficult to understand that the formation rate of •OH radicals increases with further increasing R due to the increase of the amount of surface-adsorbed TFA complexes and fluorides.

3.6. Photocatalytic activity

Fig. 10 shows the dependence of the apparent rate constants K_a of the TiO_2 samples on R. Pure TiO_2 sample prepared without TFA shows good photocatalytic activity and its K_a value reaches 4.24. This is associated with its large specific surface area, bimodal mesoporous size distribution and anatase phase structures. With increasing R, the photocatalytic activity of the TiO_2 hollow spheres is obviously enhanced and is higher than that of TiO_2 solid spheres due to the enhancement of TiO_2 crystallization, formation of hollow structures and surface fluorination of TiO_2 via TFA and F^-. At $R = 2$, the sample shows the highest photocatalytic activity and its K_a is 6.58. This superior photocatalytic activity is attributed to an optimal concentration of surface-bound CF_3COO^- and F^- anions. However, the photocatalytic activity decreases when R is further increased. This result implies that the photocatalytic activity strongly depends on the concentration of trifluoroacetate and F^- complexed on the TiO_2 surface because the trifluoroacetate complex and F^- can serve not only as a mediator of interfacial charge transfer but also as a recombination center. Our previous results also indicate that high fluoride concentrations are not suitable for the enhancement of photocatalytic activity [22,37]. In this study, an optimal R is 2. When R is above 2, CF_3COO^- and F^- ions steadily become recombination centers and the activity decreases. On the contrary, with increasing R, the formation rates of •OH radicals on the surface of UV-illuminated TFA-TiO_2 hollow spheres always increase. This indicates that the formation rate of •OH radicals during photocatalysis is not in agreement with the photocatalytic activity [37], implying that the method of the above •OH radicals detected is not suitable for gaseous photocatalytic reactions. Another possible explanation is that the formation rate of •OH radicals is an important factor influencing photocatalytic activity, but is not the only factor. Some other factors such as specific surface areas, pore structures, crystallinity and the modifier concentration also have a great influence on photoactivity [67,68]. Of course, further work is required to address this difference and its mechanism [37].

We also investigated the photocatalytic activity of the TFA-TiO_2 hollow spheres for the photocatalytic degradation of Rhodamine B (RhB) in water in order to demonstrate their potential application for water purification. The characteristic absorption peak of RhB at 553 nm was used to monitor the photocatalytic degradation process [69]. The results showed that the absorption peak at 553 nm dropped rapidly with increasing UV exposure time and almost disappeared after 1 h (not shown here), indicating the complete photocatalytic decolorization of RhB aqueous solution during the reaction, also the $R = 2$ samples having higher photocatalytic activity than P25. Further experiments indicated that the hollow spheres could be more readily separated from the slurry system by filtration or sedimentation after photocatalytic reaction and reused than nano-sized P25 powder photocatalytic materials due to their large weight, weak Brownian motion and good mobility [69]. After five recycles for the photodegradation of RhB, the catalyst did not exhibit any significant loss of activity and changes of morphology, confirming the TiO_2 hollow spheres with good stability and mechanical strength. Therefore, the prepared TiO_2 hollow spheres can be regarded as an ideal photocatalyst for environmental purification. We believe that the prepared TiO_2 hollow spheres are also of great interest in catalysis, solar cell, separation technology, biomedical engineering and nanotechnology.

4. Conclusion

TFA and F^- modified TiO_2 hollow microspheres with highly photocatalytic activity are synthesized by one-pot hydrothermal treatment of $Ti(SO_4)_2$ solution in the presence of trifluoroacetic acid. High-temperature hydrothermal environment results in the decomposition of TFA, thus production of F^-. CF_3COO^- and F^- induce the formation of hollow structure and adsorb on the surface of TiO_2. R displays a great influence on the photocatalytic activity

and microstructures of mesoporous TiO_2 hollow spheres. The photocatalytic activity of all TFA-TiO_2 hollow spheres is higher than that of P25 and pure TiO_2. At $R = 2$, the photocatalytic activity of TFA-TiO_2 hollow spheres reaches the highest and exceeds that of P25 by a factor of more than two times. This is due to the fact that an optimal TFA concentration is beneficial to reduce the recombination of photo-generated electrons and holes, also the hollow nanostructure can enhance the transfer and transport of charge carriers and reactant and product molecules. When R is above 2, CF_3COO^- and F^- ions steadily become recombination centers of photo-generated electrons and holes and the activity decreases.

Acknowledgements

This work was partially supported by the National Natural Science Foundation of China (50625208, 20773097 and 20877061). This work was also financially supported by the National Basic Research Program of China (2007CB613302 and 2009CB939704).

References

[1] A. Fujishima, K. Honda, Nature 238 (1972) 37–38.
[2] M.R. Hoffmann, S.T. Martin, W. Choi, D.W. Bahnemann, Chem. Rev. 95 (1995) 69–96.
[3] L.G. Devi, N. Kottam, S.G. Kumar, J. Phys. Chem. C 113 (2009) 15593–15601.
[4] L.G. Devi, B.N. Murthy, S.G. Kumar, Chemosphere 76 (2009) 1163–1166.
[5] C. Trapalis, N. Todorova, M. Anastasescu, C. Anastasescu, M. Stoica, M. Gartner, M. Zaharescu, T. Stoica, Thin Solid Films 517 (2009) 6243–6247.
[6] L.S. Zhang, K.H. Wong, Z.G. Chen, J.C. Yu, J.C. Zhao, C. Hu, C.Y. Chan, P.K. Wong, Appl. Catal. A 363 (2009) 221–229.
[7] J.G. Yu, Y.R. Su, B. Cheng, Adv. Funct. Mater. 17 (2007) 1984–1990.
[8] X.X. Yu, J.G. Yu, B. Cheng, M. Jaroniec, J. Phys. Chem. C 113 (2009) 17527–17535.
[9] J.G. Yu, Q.J. Xiang, M.H. Zhou, Appl. Catal. B 90 (2009) 595–602.
[10] S.W. Liu, J.G. Yu, S. Mann, J. Phys. Chem. C 113 (2009) 10712–10717.
[11] Y.X. Li, G.X. Lu, S.B. Li, J. Photochem. Photobiol. A 152 (2002) 219–228.
[12] J.H. Park, S. Kim, A.J. Bard, Nano Lett. 6 (2006) 24–28.
[13] J.G. Yu, H.G. Yu, B. Cheng, X.J. Zhao, J.C. Yu, W.K. Ho, J. Phys. Chem. B 107 (2003) 13871–13879.
[14] M. Ksibi, S. Rossignol, J.M. Tatibouet, C. Trapalis, Mater. Lett. 62 (2008) 4204–4206.
[15] S.N. Frank, A.J. Bard, J. Am. Chem. Soc. 99 (1977) 303–308.
[16] L.G. Devi, B.N. Murthy, S.G. Kumar, J. Mol. Catal. A 308 (2009) 174–181.
[17] H. Park, W. Choi, J. Phys. Chem. B 108 (2004) 4086–4093.
[18] W. Choi, Catal. Surv. Asia 10 (2006) 16–28.
[19] P.V. Kamat, Chem. Rev. 93 (1993) 267–269.
[20] M.S. Vohra, S. Kim, W. Choi, J. Photochem. Photobiol. A 160 (2003) 55–60.
[21] S.N. Subbarao, Y.H. Yun, R. Kershaw, K. Dwight, A. Wold, Inorg. Chem. 18 (1979) 488–492.
[22] J.C. Yu, J.G. Yu, W.K. Ho, Z.T. Jiang, L.Z. Zhang, Chem. Mater. 14 (2002) 3808–3816.
[23] J.G. Yu, J.C. Yu, B. Cheng, S.K. Hark, K. Iu, J. Solid State Chem. 174 (2003) 372–380.
[24] A. Hattori, M. Yamamoto, H. Tada, S. Ito, Chem. Lett. 27 (1998) 707–708.
[25] A. Hattori, K. Shimoda, H. Tada, S. Ito, Langmuir 15 (1999) 5422–5425.
[26] C.M. Wang, T.E. Mallouk, J. Phys. Chem. 94 (1990) 423–428.
[27] C.M. Wang, T.E. Mallouk, J. Phys. Chem. 94 (1990) 4276–4280.
[28] J.C. Yu, W.K. Ho, J.G. Yu, S.K. Hark, K. Iu, Langmuir 19 (2003) 3889–3896.
[29] C. Minero, G. Mariella, V. Maurino, E. Pelizzetti, Langmuir 16 (2000) 2632–2641.
[30] C. Minero, G. Mariella, V. Maurino, D. Vione, E. Pelizzetti, Langmuir 16 (2000) 8964–8972.
[31] J.S. Park, W. Choi, Langmuir 20 (2004) 11523–11527.
[32] M. Lewandowski, D.F. Ollis, J. Catal. 217 (2003) 38–46.
[33] H. Kim, W. Choi, Appl. Catal. B 69 (2007) 127–132.
[34] J. Ryu, W. Choi, Environ. Sci. Technol. 38 (2004) 2928–2933.
[35] J.S. Park, W. Choi, Chem. Lett. 34 (2005) 1630–1631.
[36] Y.M. Xu, K.L. Lv, Z.G. Xiong, W.H. Leng, W.P. Du, D. Liu, X.J. Xue, J. Phys. Chem. C 111 (2007) 19024–19032.
[37] J.G. Yu, W.G. Wang, B. Cheng, B.L. Su, J. Phys. Chem. C 113 (2009) 6743–6750.
[38] P. Wardman, J. Phys. Chem. 18 (1989) 1637–1735.
[39] J.M. Macak, H. Tsuchiya, P. Schmuki, Angew. Chem. Int. Ed. 44 (2005) 2100–2102.
[40] Y.W. Jun, M.F. Casula, J.H. Sim, S.Y. Kim, J.W. Cheon, A.P. Alivisatos, J. Am. Chem. Soc. 125 (2003) 15981–15985.
[41] K. Kanie, T. Sugimoto, Chem. Commun. 14 (2004) 1584–1585.
[42] J.G. Yu, W. Liu, H.G. Yu, Cryst. Growth Des. 8 (2008) 930–934.
[43] F. Caruso, R.A. Caruso, H. Mohwald, Science 282 (1998) 1111–1114.
[44] A. Imhof, Langmuir 17 (2001) 3579–3585.
[45] H.G. Yang, H.C. Zeng, J. Phys. Chem. B 108 (2004) 3492–3495.
[46] Y.D. Yin, R.M. Rioux, C.K. Erdonmez, S. Hughes, G.A. Somorjai, A.P. Alivisatos, Science 304 (2004) 711–714.
[47] H.G. Yang, H.C. Zeng, Angew. Chem. Int. Ed. 43 (2004) 5930–5933.
[48] J.G. Yu, H.T. Guo, S.A. Davis, S. Mann, Adv. Funct. Mater. 16 (2006) 2035–2041.
[49] J.G. Yu, H.G. Yu, H.T. Guo, M. Li, S. Mann, Small 4 (2008) 87–91.
[50] J.G. Yu, S.W. Liu, H.G. Yu, J. Catal. 249 (2007) 59–66.
[51] D.Y. Zhang, D. Yang, H.J. Zhang, C.H. Lu, L.M. Qi, Chem. Mater. 18 (2006) 3477–3485.
[52] Z.Y. Liu, D.D. Sun, P. Guo, J.O. Leckie, Chem. Eur. J. 13 (2007) 1851–1855.
[53] X.W. Lou, L.A. Archer, Z.C. Yang, Adv. Mater. 20 (2008) 3987–4019.
[54] K.S.W. Sing, D.H. Everett, R.A.W. Haul, L. Moscou, R.A. Pierotti, J. Rouquerol, T. Siemieniewska, Pure Appl. Chem. 57 (1985) 603–619.
[55] K. Ishibashi, A. Fujishima, T. Watanabe, K. Hashimoto, Electrochem. Commun. 2 (2000) 207–210.
[56] Q. Xiao, Z.C. Si, J. Zhang, C. Xiao, X.K. Tan, J. Hazard. Mater. 150 (2008) 62–67.
[57] J.G. Yu, G.H. Wang, B. Cheng, M. Zhou, Appl. Catal. B 69 (2007) 171–180.
[58] J.G. Yu, J.C. Yu, M.K.P. Leung, W. Ho, B. Cheng, X. Zhao, J. Zhao, J. Catal. 217 (2003) 69–78.
[59] Q. Peng, S. Xu, Z. Zhuang, X. Wang, Y. Li, Small 1 (2005) 216–221.
[60] S. Nishimura, N. Abrams, B.A. Lewis, L.I. Halaoui, T.E. Mallouk, K.D. Benkstein, J. van de Lagemaat, A.J. Frank, J. Am. Chem. Soc. 125 (2003) 6306–6310.
[61] S.W. Liu, J.G. Yu, S. Mann, Nanotechnology 20 (2009) 325606–325613.
[62] X.X. Yu, J.G. Yu, B. Cheng, B.B. Huang, Chem. Eur. J. 15 (2009) 6731–6739.
[63] J.G. Yu, X.J. Zhao, Q.N. Zhao, Thin Solid Films 379 (2000) 7–14.
[64] J.G. Yu, X.J. Zhao, Q.N. Zhao, Mater. Chem. Phys. 69 (2001) 25–29.
[65] C. Trapalis, V. Kozhukharov, B. Samuneva, P. Stefanov, J. Mater. Sci. 28 (1993) 1276–1282.
[66] J.G. Yu, Y.R. Su, B. Cheng, M.H. Zhou, J. Mol. Catal. A 258 (2006) 104–112.
[67] J.G. Yu, Q.J. Xiang, J.R. Ran, S. Mann, CrystEngComm 12 (2010) 872–879.
[68] B. Cheng, Y. Le, J.G. Yu, J. Hazard. Mater. 177 (2010) 971–977.
[69] J.G. Yu, X.X. Yu, Environ. Sci. Technol. 42 (2008) 4902–4907.